Evaluation of Remote Sensing Techniques for Lithological Mapping in the Southeastern Pamir using Landsat 8 OLI Data

Aminov Javhar,[1,2,3] Xi Chen,[1,2,4] Aminov Jovid,[2,3] Mamadjanov Yunus,[3,4] Aminov Jamshed,[2,5] Duulatov Eldiiar [1,2] And Bakhtiyorov Zulfiyor [1,2]

[1]State Key Laboratory of Remote Sensing and GIS, Xinjiang Institute of Ecology & Geography, Chinese Academy of Sciences, Urumqi 830011, China, E-mail: javhar_85@mails.ucas.ac.cn, e.duulatov@mail.ru, zulfiyor@mail.ru

[2]University of Chinese Academy of Sciences, Beijing 100049, China, E-mail: chenxi@ms.xjb.ac.cn

[3]Institute of Geology, Earthquake Engineering and Seismology, Tajikistan Academy of Sciences, Dushanbe 735823, Tajikistan, E-mail: jovid.aminov@outlook.com

[4]Research Center for Ecology and Environment of Central Asia (Dushanbe), Dushanbe 735823, Tajikistan E-mail: petrology@mail.ru

[5]Key Laboratory of Continental Collision and Plateau Uplift, Institute of Tibetan Plateau Research, Center for Excellence in Tibetan Plateau Earth Sciences, Chinese Academy of Sciences, Beijing 100101, China E-mail: aminov.j.sr@gmail.com

Abstract

In this study, we test the Landsat 8 OLI data potential for lithological mapping in the Southeastern Pamir. Discrimination of lithological units in the study area has been carried out by utilizing Landsat 8 OLI Satellite data and image enhancement techniques. The approaches consist of spectral enhancement such as independent component analysis (ICA), band ratioing, and false-color composition (FCC). The spectral enhancement techniques were applied in order to extract the initial lithological information, which shows a clear discrimination of granitic rocks from terrigenous and carbonate sedimentary successions. FCC image (OLI bands 6, 7 and 5), color-ratio composite image (OLI 6/5, OLI (7x5)/7, and OLI 6/7), and color composite of independent components (IC6, IC3, IC4) in red, green and blue respectively were found as combinations with more contrast on lithologic information and were used as the input data in supervised classification. Maximum likelihood classification was used to classify resultant images. The results, verified with field observations, demonstrate that different kind of granitoids, terrigenous and carbonaceous rocks can be distinguished and delineated, leading to constriction of geological maps with a better accuracy.

1. Introduction

The satellite remotely sensed data are extremely useful for geological investigation. In the past, the geological maps were prepared from conventional ground surveys based on field observations. They are made along traverse lines at regular intervals. While plotting such point information collected along the traverse lines on the topographic base and ultimately preparing final maps by extrapolating the details, certain errors are unavoidable and lead to inaccuracies in maps. Especially in mountainous regions, where many areas are difficult to access the traditional mapping accuracy is very low.

Fortunately, remote sensing techniques have opened a new era in lithological mapping. Remote Sensing and GIS techniques can be integrated to distinguish rock types and lineaments (Ali and Ali, 2013). Furthermore, such techniques as digital image processing (DIP), image enhancements, including transformed data feature space (PCA, ICA), band ratioing, color composites (true or false), decorrelation stretch, spectral index have facilitated the differentiation, mineralization and soil application studies (Ali et al., 2012, Hung et al., 2005, Bertoldi et al., 2011, Asadzadeh and de Souza Filho, 2016, Ali, 2013 and Ninomiya and Fu, 2010).

One of the mountainous areas, which is difficult to access for ground based surveys, is Pamir. This area is a western continuation of Tibetan-Himalayan region and remains geologically least studied in this region. This is partly because of the region's topography and the climate, which make it difficult to access during ground based surveys. The geological maps plotted during ground based surveys in the 20-th century are the topic of disputes and need

to be reconstructed. Despite the Pamir is a semiarid highland without much vegetation and with good surface exposure of rocks, being an ideal place for assessing the potential of remote sensing techniques for geological mapping, it also still remains unstudied in terms of geological remote sensing.

The main objective of this study is to show the potential of application of remote sensing techniques in lithological mapping of the Alichur area, Southeastern Pamir, Tajikistan. For reaching this objective we use Landsat 8 OLI data and implement available up-to-date spatial and spectral analysis software, and finally verify our results with field observations. Our focus in this study is made on mapping the igneous rocks of the Pamir by distinguishing them from other type of rocks with use of remotely sensed data, as well as delineating different type of igneous rocks from each other.

2. Geological Setting

The Southern Pamir, a tectonic zone of the Pamir Plateau, which consists of three such zones (Northern, Central and Southern) (e.g. Aminov et al., 2017) extends from Sarez lake in the North to the Afghan-Tajik boundary in the south, and from Shahdara Range in the west to the Sarykol Range in the East (Figure 1a). It is often divided into Southwestern Pamir and Southeastern Pamir (Angiolini et al., 2013, Burtman and Molnar, 1993 and Robinson, 2015). The SW Pamir characterized by Precambrian metamorphic rocks and the SE Pamir shows a thick Permian to Cenozoic sedimentary succession, stacked into a polyphase Mesozoic-Cenozoic fold and thrust belt, which escaped the important metamorphism affecting most of the surrounding units (Angiolini et al., 2013 and Angiolini et al., 2014).

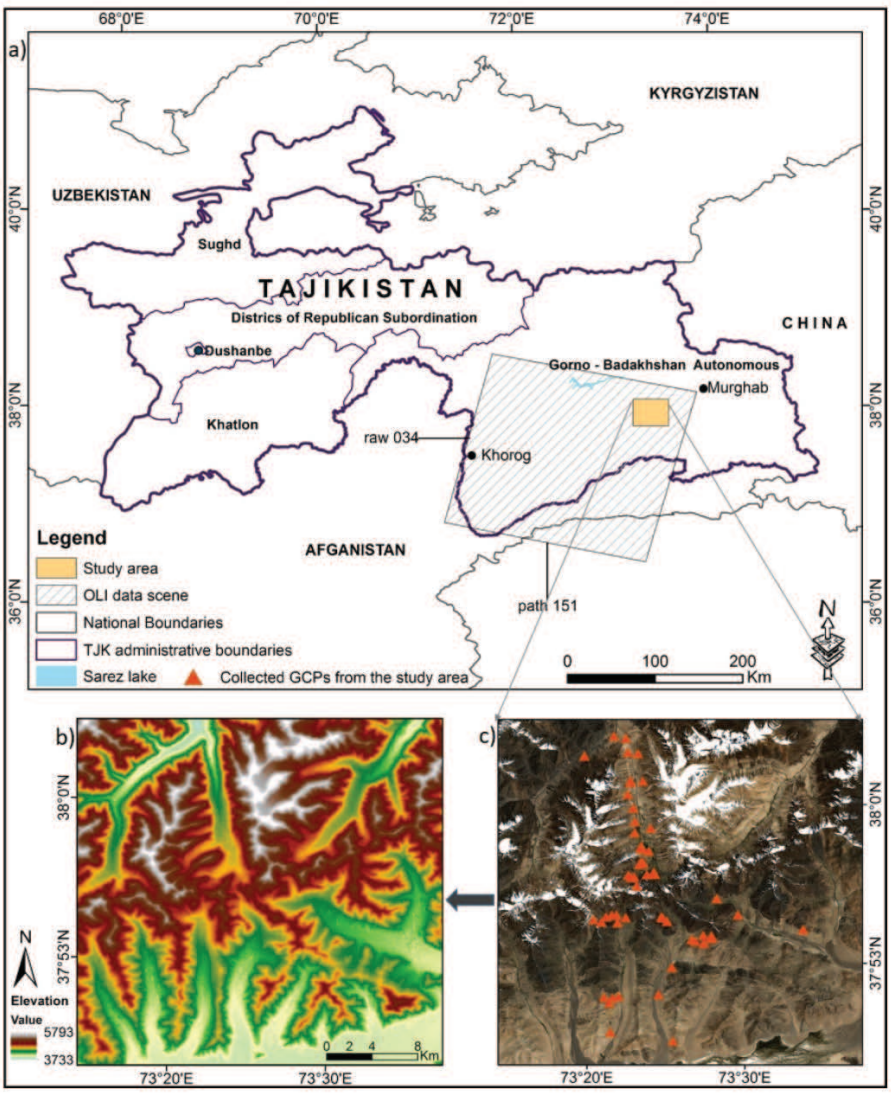

Figure 1: Location map of the study area and the Landsat 8 OLI data scene

Crystalline rocks and sedimentary deposits of the Southern Pamir are intruded by a series of Mesozoic – Cenozoic igneous plutons, which cover about 30-40% of the surface geological outcrops, and are of intermediate to felsic composition, though some mafic plutons are also present in a smaller extent. These igneous rocks are important in understanding the tectonic history of the Pamir, because they have recorded a suit of tectonic events related to suturing of the Gondwanan terrains to the southern margin of Eurasia in the Mesozoic and the collision of Indian plate with Eurasian in the Cenozoic. The Mesozoic suturing events and Cenozoic collision, followed by convergence between Indian and Asian plates have caused shortening and deformation of geological structure of the Pamir, making it difficult to study (e.g. Aminov et al., 2017, Robinson, 2015 and Stubner et al., 2013).Therefore, comprehensive study of the distribution and genesis of igneous rocks of the Pamir is crucial for understanding the tectonic history of the region. Moreover, study of distribution of different type of igneous rocks would lead to better understanding of ore-bearing potential of the region, hence providing better opportunities for discovering new mineral deposits.

For this study we have chosen an area where main types of sedimentary and igneous rocks of the region are present and are in a good interrelation with each other, making the area best for testing the potential of RS and GIS in lithological mapping. This area is located approximately 60 km southeast of Lake Sarez (Figure 1a), near the Alichur village. It is situated between the following coordinates: Latitudes 38°3′41″ N and 37°47′25″N, Longitudes 73°14′18″ E and 73°36′16″E. According to the values extracted from digital elevation model, the research area rises from 3733 m up to 5793 m above sea level (Figure 1b). Geologically, the study area comprises sedimentary rocks of terrigenous and carbonaceous composition of Permian to Jurassic age intruded by a polyphase pluton of dioritic to granitic composition (Figure 2).

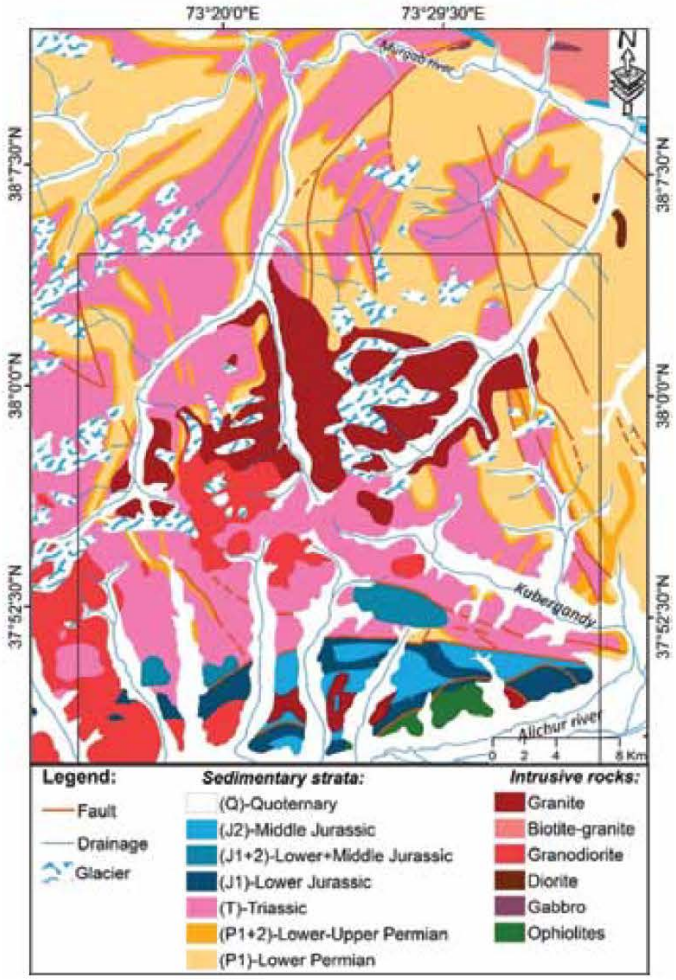

Figure 2: Simplified geologic map of Alichur area. After Denikaev (1966) and Voskonyanc (1966). Black square shows the study area

Permian rocks are represented by lower Permian slates and sandstones interlayered with some effusive rocks (P_1), and lower–upper Permian limestone, claystone and siltstone with some interlayers of tuff (P_1+_2). Triassic section begins with alternation of limestone and sandstone, however, most of the section (about 90%) is composed of black sandstone+siltstone+conglomerate. Jurassic rocks are represented by lower Jurassic sandstone and conglomerates with some limestone and marl (J_1), lower to middle Jurassic limestone and marl with some sandstone and conglomerate, and upper Jurassic sandstone and slate with thin layers of limestone (Vlasov et al., 1991). Plutonic body intruding these sedimentary sequences comprises biotite bearing diorites (granodiorite + quartz diorite of Alichur igneous complex (age: $J_3 - K_1$) and biotite + muscovite bearing granites and leucogranites of Bashgumbaz complex (age: K_2; Vladimirov et al., 1990).

3. Data and Methodology

3.1 Dataset

Landsat 8 OLI (Operational Land Imager-Thermal Infrared Sensor) imageries provide a number of bands in the visible, two SWIR and thermal infrared regions. They are available free of charge via the USGS Earth Explorer. The selection of the imagery was based on the acquisition date, availability and spatial resolution as well as the user need. Terrain corrected Landsat 8 scene (path/raw = 151/034), comprising 11 bands (coastal aerosol, blue, green, red, near infrared, two shortwave infrared, panchromatic, cirrus and two thermal infrared), free of cloud, covering the study area was downloaded from USGS Earth Explorer website. Bands 1-7 with spatial resolution of 30m were utilized in the study. The acquisition date of the provided data is 22-July-2014.

3.2 Data Pre-Processing

The Landsat OLI data cover the study area were digitally pre-processed through ENVI (5.1) software to improve the quality of the raw data. In order to get the data prepared for further digital image processing, the Landsat 8 OLI calibrated digital numbers (DNs) were converted to physical units, such as sensor radiance and surface reflectance (SR), and atmospheric correction was performed to remove or at least minimize the atmospheric effects in the raw data. Geometric correction was not necessary as the acquired satellite image was already geo-referenced in the Universal Transverse Mercator (UTM) projected coordinate system (Zone 43) based on the WGS84 datum. Further, radiometric calibration and FLAASH (Fast Line-of-Sight Atmospheric Analysis of Spectral Hypercubus) atmospheric correction model (Kaufman et al., 1997) was implemented in ENVI software with the Mid-Latitude Summer atmospheric model and the Rural aerosol model.

Since the FLAASH model produces negative minimums and multiplies reflectance by ten thousand, the gained results were converted to reflection values in the range of 0 to 1 that minimizes processing time of the imagery. The values from computed statistics before and after conversion are shown in Table 1. Hereinafter, the imagery was imported in to ERDAS Imagine 2013 software for sub-setting and band selection. Image sub-setting was performed in order to extract the targeted area and the channels needed for this study.

Table 1: Computed basic statistics of OLI image before conversion and after conversion to values (0-1)

	Min		Max		Mean		St.dev	
Band #	**Before**	**After**	**Before**	**After**	**Before**	**After**	**Before**	**After**
Band 1	-1447	0	12467	1	1030.644	0.103	1383.833	0.138
Band 2	-838	0	15191	1	1048.954	0.104	1387.316	0.138
Band 3	-779	0	12536	1	1319.931	0.131	1558.775	0.155
Band 4	-610	0	11888	1	1471.572	0.147	1622.372	0.162
Band 5	-350	0	11394	1	1661.211	0.166	1538.490	0.153
Band 6	-75	0	12598	1	1439.169	0.143	1410.002	0.141
Band 7	-40	0	12464	1	1233.908	0.123	1216.822	0.121

3.3 Data Processing

The image processing implemented in this study includes building False Color Composite (FCC) image, Independent Component Analysis (ICA) and band ratioing analysis. For FCC image bands 5, 6 and 7 are found to be more informative for lithological delineation than bands 1, 2, 3 and 4. ICA is a feature extraction technique which aims to find a set of uncorrelated components being as independent as possible from each other (Jutten and Herault, 1991, Cruces-alvarez et al., 2004, Yang and Cheng, 2014a and Mi, 2014). Each component contains spectral information corresponding to a specific feature in the original image. In comparison to PCA, the ICA has been proved to be more applicable for characterization as well as for classification of lithological units (Yang and Cheng, 2014b). Band ratioing was applied to extract and emphasize differences in spectral reflectance of materials and subdues the topographic and shadow effects. Ratio images are prepared by dividing the DN value in one band by the corresponding DN value in another band for each pixel where the resulting DN values represent the ratio image. Ratio images can be displayed as grey scale or color composite image. In addition to the use of ratio images separately, they can also be used to generate false color composite (FCC) image by combining three monochromatic ratio data sets (Sultan et al., 1987). Such composite has a two-fold advantage of combining data from more than two bands and presenting the data in color, which further facilitates the interpretation of subtle spectral reflectance differences (Qari, 2011).

Several color composite images have been performed using combinations of different ratios of OLI bands to select the optimum combination most helpful in the lithological discrimination of the study area.

3.4 Image Classification

The supervised classification involves a considerable amount of input from the image analysis and knowledge of the types of surface that are found in the study area. This information can be obtained from existing maps or from the actual field works where different surface classes are identified and their geographical positions can be noted (Amri et al., 2011 and Chen and Zhou, 2015). Therefore, field observation was conducted in 14 days for ground verification and 58 Ground Control Points (GCPs) were collected using a Global Positioning System (GPS) which is used to confirm the spatial accuracy of the satellite imagery. The locations of collected GCPs are shown in Figure 1c. The maximum likelihood classification (MLC) widely used in geological studies was applied to the resultant color composite images from ICA and band ratios. Separability analysis was performed in signature files using ArcGIS 10.3 to select the best training signatures for the supervised classification. A confusion matrix was carried out to assess the accuracy of classification results (Duulatov et al., 2016), using ground verification information collected based on the field truthing.

4. Results and Discussion

According to spectral characteristics extracted from the utilized image (Figure 3), the best lithological contrast appears to be displayed by the color composition of bands 6, 7 and 5 in RGB respectively. As it is demonstrated on Figure 4, this band combination allows delineation of granitic and dioritic bodies by their bright colors; sedimentary carbonate rocks also have bright color, which well distinguishes them from terrigenous rocks. The results of loadings on ICs obtained by ICA (Table 2) and the interpreted geological objects from these ICs (Figure 5a) demonstrate that the individual components # 3, 4 and 6 can be interpreted to be associated with certain lithological units within the study area. For example, granites are distinguished on IC3 by their positive values whereas dioritic rocks and Jurassic carbonaceous rocks (J1+2; indicated as Jc in the table and the figures) are distinguished by negative values (Figure 5b).

Similarly, the IC4 distinguishes the Jurassic terrigenous rocks (Jt) by their positive values and dioritic rocks by their negative values (Figure 5c). Jurassic carbonaceous and Permian to Jurassic terrigenous rocks (P-Jt) can be best discriminated from the igneous rocks on IC6 by their respectively positive and negative values (Figure 5d). An FCC image from these independent components was made by assigning IC6 to red, IC3 to green and IC4 to blue components of RGB (Figure 6). This FCC image well differentiates between different rock units as it comprises most of the data reflecting lithological variations. This image proved to be significant for rock discrimination where each rock type has its specific color.

After making several color composite images from band ratios, we found band ratios combination of 6/5, (7x5)/7 and 6/7, displayed in RGB respectively (Figure 7), most suitable to discriminate igneous rocks of the study area from the sedimentary deposits. Igneous pluton, comprising diorites and granites indicate these rocks in pink and orange colors respectively on this composite image.

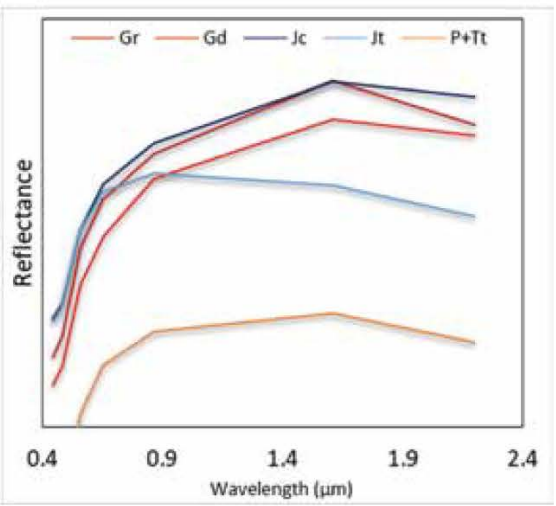

Figure 3: Spectral characteristics of different rock units in the study area extracted from OLI 8 data. Rock indexes are described in Figure 4

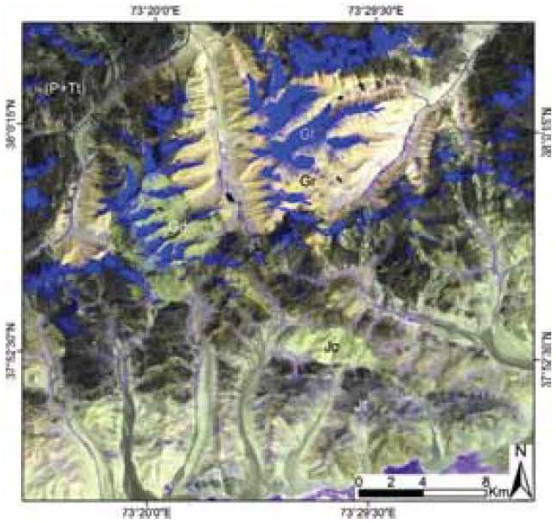

Figure 4: False color composite image. Bands 6, 7 and 5 in the RGB respectinely. Granite (Gr), Granodiorite (Gd), Jurassic carbonaceous rocks (Jc), Jurassic terrigenious rocks (Jt), Permian to Triassic terrigenious rocks (P+Tt), Glacier (Gl)

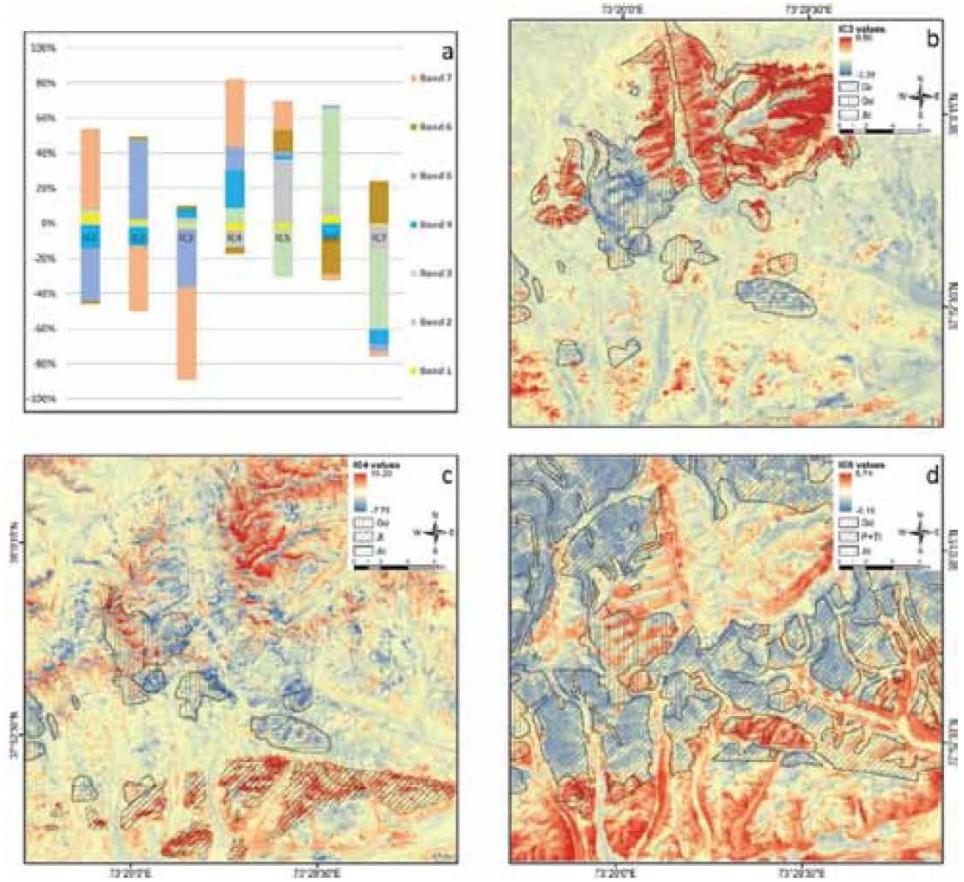

Figure 5: Results gained by ICA applied to preprocessed data: (a) 100% stacked diagram showing the loadings of elements on ICs; (b–d) maps showing values on ICs 3, 4, 6 respectively. Line patterns represent various rock units digitized from geological map of the study area. Granite (Gr), Granodiorite (Gd), Jurassic carbonaceous rocks (Jc), Jurassic terrigenous rocks (Jt), Permian to Triassic terrigenous rocks (P+Tt)

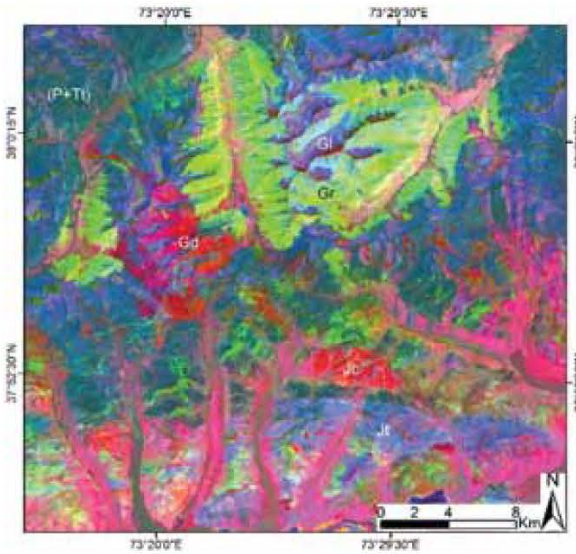

Figure 6: Color composite of independent components from ICA of Landsat 8 OLI image (IC6, IC3, IC4 in R, G, B) of the study area. Granite (Gr), Granodiorite (Gd), Jurassic carbonaceous rocks (Jc), Jurassic terrigenious rocks (Jt), Permian to Triassic terrigenious rocks (P+Tt), Glacier (Gl)

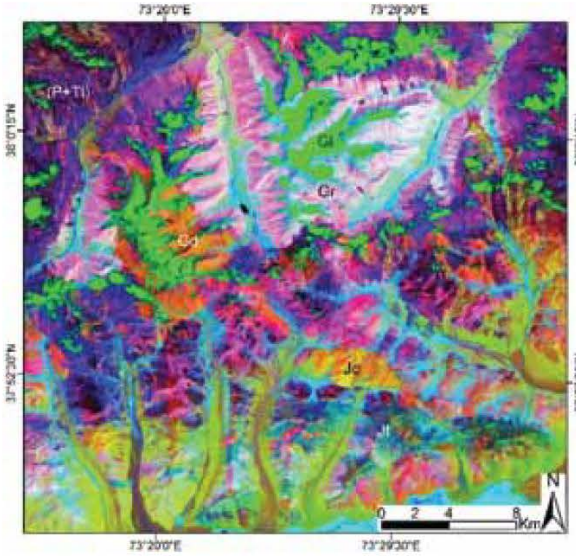

Figure 7: Landsat 8 OLI band ratio image (6/5, (7x5)/7 and 6/7 in RGB respectively). Granite (Gr), Granodiorite (Gd), Jurassic carbonaceous rocks (Jc), Jurassic terrigenious rocks (Jt), Permian to Triassic terrigenious rocks (P+Tt), Glacier (Gl)

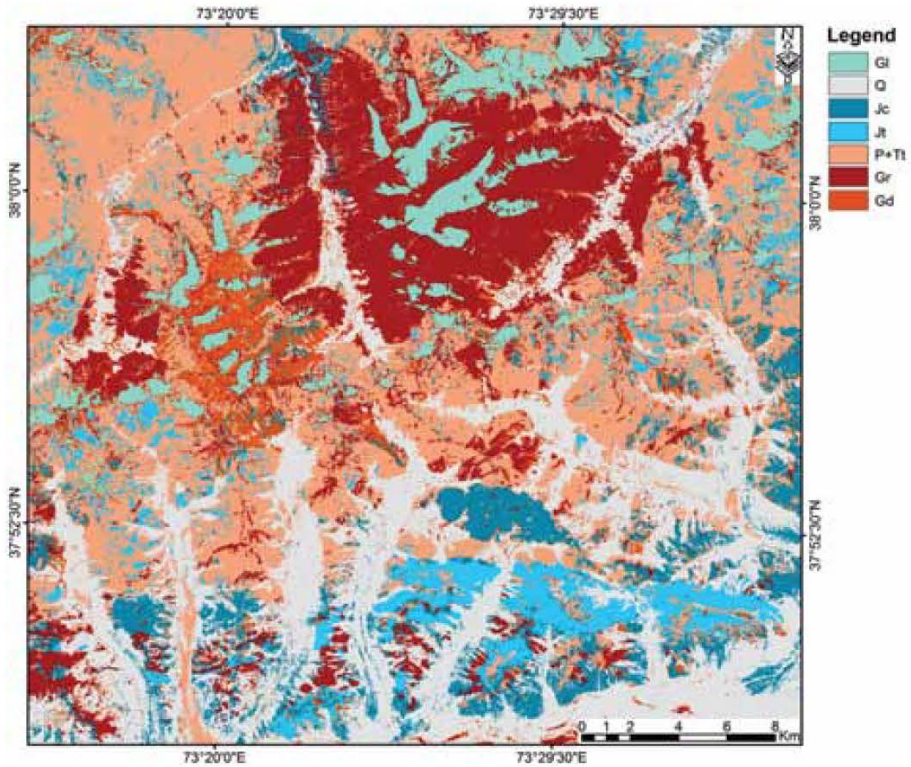

Figure 8: Lithological classification map of the Alichur area. Glacier (Gl), Quoternary (Q), Jurassic carbonaceous rocks (Jc), Jurassic terrigenious rocks (Jt), Permian to Triassic terrigenious rocks (P+Tt), Granite (Gr), Granodiorite (Gd)

Table 2: Unmixing matrix of the ICs from Independent Component Analysis. Jurassic carbonaceous rocks (Jc), Jurassic terrigenious rocks (Jt), Permian to Triassic terrigenious rocks (P+Tt)

ICs	Lithological units indicated by ICs	Band 1	Band 2	Band 3	Band 4	Band 5	Band 6	Band 7
1	None	16.38	-3.62	6.98	-38.21	-89.38	-5.13	136.54
2	None	6.32	-0.09	-6.78	-32.44	141.20	5.69	-116.42
3	Granite, Granodiorite, Jc	-3.10	8.15	-5.45	12.55	-83.94	5.21	-136.44
4	Granodiorite, Jt, Jc.	-9.94	-27.14	24.01	57.04	36.89	-10.16	105.47
5	None	-2.02	29.79	-23.01	1.69	2.05	9.70	13.50
6	Granodiorite, P+Tt and Jc	4.48	7.49	66.11	-9.86	2.04	-24.19	-4.52
7	None	-1.63	-19.72	-67.83	-12.22	-6.18	35.76	-4.576

Table 3: Confusion matrix of User's, producer's accuracies and Kappa coefficient of the supervised classification image of the reference data. Jurassic carbonaceous rocks (Jc), Jurassic terrigenious rocks (Jt), Permian to Triassic terrigenious rocks (P+Tt)

	(1)	(2)	(3)	(4)	(5)	(6)	(7)	Row Total	User's Acc. %	Commission Error %
Granite (1)	**28**	1	0	1	0	0	0	30	93.3	6.7
Granodiorite (2)	0	**26**	3	0	0	1	1	31	83.9	16.1
Jc (3)	0	0	**23**	0	0	0	2	27	85.2	14.8
Jt (4)	0	0	0	**28**	7	0	0	35	80	20
P+Tt (5)	1	0	0	0	**23**	0	1	25	92	8
Glaciers (6)	0	0	0	0	0	**29**	0	29	100	0
Quoternary (7)	0	2	4	1	0	0	**26**	33	78.8	21.2
Column total	29	31	30	30	30	30	30	**210**	**Correct points: 183**	
Producer's Acc. %	96.6	83.9	76.7	93.3	76.7	96.7	86.7	**Overall Accuracy: 87.2 %**		
Omission Error %	3.4	16.1	23.3	6.7	23.3	3.3	13.3	**Kappa Statistic: 85 %**		

The data processing results used for implementation of supervised maximum likelihood classification resulted in utilization of seven lithological classes representing Granite, Granodiorite, Jurassic carbonates, Jurassic sedimentary rocks, Quoternary deposits and Glaciers. The results of this classification are shown on Figure 8. The classification demonstrates a good discrimination of igneous plutonic rocks from sedimentary deposits. Moreover, this classification also allows us to clearly distinguish between intrusive rocks of dioritic and granitic composition. Furthermore, as it is seen on the final lithological map (Figure 8) smaller granitic bodies which were not mapped during ground-based mapping surveys, are identified on processed satellite image and classified on the lithological map. This technique allows us to map lithological units with a better accuracy and resolution.

An overall accuracy of 87.2 % and a kappa statistic of 85 % were resulted. In terms of producer's accuracy, all classes were over 80 % correct with the exception of Jurassic carbonaceous rocks, which were 76.7 % respectively (Table 3).

5. Conclusions

This study allowed us to test a satellite data processing technique for lithological mapping of an area in the Southern Pamir, a western continuation of Tibetan-Himalayan orogen. The results of data processing and image classification have been verified by a fieldwork and geological map of the studied area with a scale of 1:200,000 (Denikaev, 1966 and Voskonyanc, 1966). False Color composite image (6, 7 and 5), band ratio images (OLI 6/5, OLI (7x5)/7 and OLI 6/7) and the color composite image of independent components (IC6, IC3 and IC4) provide excellent distinction between the igneous and sedimentary rocks, and even between different type of igneous rocks in the study area. Implemented on the resulted processed images, supervised maximum likelihood classification allowed us to identify seven lithological classes of sedimentary and igneous rocks, as well as glaciers. This classification demonstrates that the technique used in this study

allows differentiation of granitic rocks not only from sedimentary deposits, but also from diorites. Our results also allowed us to map smaller granitic bodies which were not mapped during ground-based mapping surveys, and identification of these small granitic bodies on the satellite image was verified to be reliable by our field observations in the study area. This work allows us to improve the accuracy of existing geological maps which were created during traditional ground-based mapping surveys in the middle of 20th century.

Acknowledgements

This study is a part of PhD research of Javhar Aminov and has been sponsored by CAS-TWAS President's Fellowship for International PhD Students awarded to him. Furthermore, the work was supported by the National Natural Science Foundation of China (Grant No. 41361140361 and 41761144079).

Reference

Ali, E. A., El Khidir, S. O., Babikir, I. A. A. and Abdelrahman, E. M., 2012, Landsat ETM + 7 Digital Image Processing Techniques for Lithological and Structural Lineament Enhancement : Case Study around Abidiya Area, Sudan. *The Open Remote Sensing Journal.* Vol. 5, No. 1, 83-89. doi:10.2174/1875413901205010083.

Ali, S. A. and Ali, U., 2013, Litho-Structural Mapping of Sind Catchment (Kashmir Basin), NW Himalaya, using Remote Sensing and GIS Techniques. *International Journal of Science and Research (IJSR).* Vol. 4, No. 7, 1325-1330.

Aminov, J., Ding, L., Mamadjonov, Y., Dupont-Nivet, G., Aminov, J., Zhang, L. Y., Yoqubov, S., Aminov, J. and Abdulov, S., 2017, Pamir Plateau Formation and Crustal Thickening before the India-Asia Collision Inferred from Dating and Petrology of the 110-92 Ma Southern Pamir Volcanic Sequence. *Gondwana Research*, Vol. 51, 310-326. doi: 10.1016/j.gr.2017.08.003.

Amri, K., Mahdjoub, Y. and Guergour, L., 2011. Use of Landsat 7 ETM+ for Lithological and structural Mapping of Wadi Afara Heouine Area (Tahifet-Central Hoggar, Algeria). *Arabian Journal of Geosciences.* Vol. 4 (7-8). 1273-1287. doi:10.1007/s12517-010-0180-8.

Angiolini, L., Zanchi, A., Zanchetta, S., Nicora, A., Vuolo, I., Berra, F., Henderson, C., Malaspina, N., Rettori, R., Vachard, D. and Vezzoli, G., 2014, From Rift to Drift in South Pamir (Tajikistan): Permian Evolution of a Cimmerian Terrane. *Journal of Asian Earth Sciences.* Vol. 102. 146-169. doi:10.1016/j.jseaes.2014.08.001.

Angiolini, L., Zanchi, A., Zanchetta, S. and Nicora, A., 2013, The Cimmerian Geopuzzle : New Data from South Pamir. *Terra Nova*, Vol. 25, No. 5, 352–360. doi:10.1111/ter.12042.

Asadzadeh, S. and de Souza Filho, C. R.,2016, A Review on Spectral Processing Methods for Geological Remote Sensing. *International Journal of Applied Earth Observations and Geoinformation.* Vol. 47. 69-90. doi:10.1016/j.jag.2015.12.004.

Bertoldi, L., Massironi, M., Visonà, D., Carosi, R., Montomoli, C., Gubert, F., Naletto, G. and Pelizzo, M. G., 2011, Mapping the Buraburi Granite in the Himalaya of Western Nepal : Remote Sensing Analysis in a Collisional Belt with Vegetation Cover and Extreme Variation of Topography. *Remote Sensing of Environment.* Vol. 115, No. 5, 1129-1144. doi:10.1016/j.rse.2010.12.016.

Burtman, V. S. and Molnar. P., 1993. Geological and Geophysical Evidence for Deep Subduction of Continental Crust Beneath the Pamir. *Geological Society of America.* Vol. 281. DOI: https://doi.org/10.1130/SPE281

Chen, X. and Zhou, Q., 2015, Ecological and Environmental Remote Sensing in Arid Zone. *Science Press*, 168.

Cruces-Alvarez, S. A., Cichocki, A. and Amari, S., 2004, From Blind Signal Extraction to Blind Instantaneous Signal Separation: Criteria, Algorithms, and Stability. *IEEE Transactions on Neural Networks*, Vol. 15(4), 859-873.

Denikaev, S. S., 1966, Geological map of the USSR (Sheet # J-43-XX, XXVI), scale 1:200000.

Duulatov, E., Chen, X., Kurban, A., Ndayisaba, F. and Monoldorova, A., 2016, Detecting Land Use/Land Cover using Landsat Imagery: Jumgal District, Kyrgyzstan. *International Journal of Geoinformatics,* Vol. 12, No. 4, 1-7.

Hung, L. Q., Batelaan, O. and De Smedt, F., 2005, Lineament Extraction and Analysis, Comparison of LANDSAT ETM and ASTER Imagery. Case Study: Suoimuoi Tropical Karst Catchment, Vietnam. *Proceedings of SPIE - The International Society for Optical Engineering.* Vol, 5983, 1-12. doi:10.1117/12.627699.

Jutten, C. and Herault, J., 1991, Blind Separation of Sources, Part I. An Adaptive Algorithm Based on Neuromimetic Architecture, *Signal Processing.* Vol. 24(1), 1-10.

Kaufman, Y. J, Wald, A.. E., Remer, L. A., Gao, B. C., Li, R. R. and Flynn, L., 1997. The MODIS 2.1- M Channel - Correlation with Visible Reflectance for use in Remote Sensing of Aerosol. *IEEE Transactions on Geoscience and Remote*

Sensing. Vol. 35(5): 1286-1298.

Mi, J. X., 2014, A Novel Algorithm for Independent Component Analysis with Reference and Methods for Its Applications. *PLoS ONE*. 9 (5): e93984. doi:10. 1371/journal.pone.0093984.

Ninomiya, Y. and Fu, B., 2010, Regional Scale Lithologic Mapping in Western Tibet using ASTER Thermal Infrared Multispectral Data. *International Archives of the Photogrammetry, Remote Sensing and Spatial Information Sciences - ISPRS Archives* 38: 454-458.

Qari, M. H. T., 2011, Utilizing Image Processing Techniques in Lithologic Discrimination of Buwatah Area, Western Arabian Shield, *Arabian Journal of Geosciences*. Vol. 4, 13-24. doi:10.1007/s12517-009-0049-x.

Robinson, A. C., 2015, Mesozoic Tectonics of the Gondwanan Terranes of the Pamir Plateau. *Journal of Asian Earth Sciences*, Vol. 102, 170-179. https://doi.org/10.1016/j.jseaes.2014.09.012.

Stubner, K., Ratschbacher, L., Rutte, D., Stanek, K., Minaev, V., Wiesinger, M. and Gloaguen, R. 2013, The Giant Shakhdara Migmatitic Gneiss Dome, Pamir, India-Asia Collision Zone: 1. Geometry and Kinematics. *Tectonics*, Vol. 32(4), 948-979. https://doi.org/10.1002/tect.20057.

Sultan, M., Arvidson, R. E., Sturchio, N. C. and Guinness, E. A., 1987, Lithologic Mapping in Arid Regions with Landsat Thematic Mapper Data: Meatiq Dome, Egypt. *Geological Society of America Bulletin*. Vol. 99, No. 6, 748-762 . doi:10.1130/0016-7606(1987)99<748:LMIARW>2.0.CO;2.

Vladimirov, A. G., Belyaeva, R. T. and Ponomarchuk, V. A., 1990, Late Mesozoic Magmatism of South Pamir. Granitic Magmatism and Mineralization of Bazardara Mining District (South-East Pamir), Novosibirsk, Institute of Geology and Geophysics of Siberian branch of the Russian Academy of Sciences: 19-69.

Vlasov, N., Dyakov, Y. A. and Cherev, E., 1991, Geological Map of the Tajik SSR and Adjacent Territories, 1: 500,000. Leningrad: VSEGEI.

Voskonyanc, G. S., 1966, Geological Map of the USSR (sheet # J-43-XIV), scale 1:200000.

Yang, J. and Cheng, Q., 2014a, A Comparative Study of Independent Component Analysis with Principal Component Analysis in Geological Objects Identification. Part II: A Case Study of Pinghe District, Fujian, China. *Journal of Geochemical Exploration*. Vol. 149, 136-146. doi:10.1016/j.gexplo.2014.11.014.

Yang, J. and Cheng, Q., 2014b, A Comparative Study of Independent Component Analysis with Principal Component Analysis in Geological Objects Identification, Part I: Simulations. *Journal of Geochemical Exploration*. Vol. 149, 127-135. doi:10.1016/j.gexplo.2014.11.